© Indian Academy of Sciences

Review

Neutron Stars: Laboratories for Fundamental Physics Under Extreme Astrophysical Conditions

DEBADES BANDYOPADHYAY[1,2]

[1]Astroparticle Physics and Cosmology Division, Saha Institute of Nuclear Physics, 1/AF Bidhannagar, Kolkata 700 064, India.
[2]Homi Bhabha National Institute, Training School Complex, Anushaktinagar, Mumbai 400 094, India.
E-mail: debades.bandyopadhyay@saha.ac.in

Abstract. We discuss different exotic phases and components of matter from the crust to the core of neutron stars based on theoretical models for equations of state relevant to core collapse supernova simulations and neutron star merger. Parameters of the models are constrained from laboratory experiments. It is observed that equations of state involving strangeness degrees of freedom such as hyperons and Bose–Einstein condensates are compatible with $2M_{\text{solar}}$ neutron stars. The role of hyperons is explored on the evolution and stability of the protoneutron star in the context of SN1987A. Moment of inertia, mass and radius which are direct probes of neutron star interior are computed and their observational consequences are discussed. We continue our study on the dense matter under strong magnetic fields and its application to magnetoelastic oscillations of neutron stars.

Keywords. Neutron stars—equations of state—magnetic fields.

1. Introduction

James Chadwick wrote to Niels Bohr about the discovery of the neutron in a letter dated 24 February 1932 (Yakovlev *et al.* 2013). The paper on the discovery of the neutron was published in *Nature* on 27 February 1932. It is amazing to note that Lev Landau thought of a highly dense astrophysical object as a giant nucleus in 1931 well before this discovery and wrote an article on this subject which was published almost at the same time of the discovery of the neutron on 29 February 1932 (Landau 1932). In the Stanford meeting of the American Physical Society in 1933, Baade & Zwicky (1934) declared: "With all reserve we advance the view that supernovae represent the transition from ordinary stars to neutron stars which in their final stages consist of extremely closely packed neutrons." These developments marked the beginning of research in physics and astrophysics of neutron stars (Yakovlev *et al.* 2013).

Shortly after the discovery of a pulsar in 1967 (Hewish *et al.* 1968), the study of dense matter in the core of neutron stars gained momentum. With the advent of X-ray, gamma-ray and radio telescopes, the observational study of neutron stars has entered into a new era. Space-based Indian Observatory AstroSat is the newest addition in this pool. Observations using these facilities as well as other telescopes are pouring in very exciting data on neutron stars. From those observations, it might be possible to estimate masses, radii, moment of inertia, surface temperatures and magnetic fields of neutron stars (Konar *et al.* 2016). The next generation radio telescope known as the Square Kilometer Array (SKA) is to be co-located in South Africa and Australia. With the detection of gravitational wave signal from the event in GW150914 by LIGO Observatory, gravitational wave astrophysics opens a new window to probe the neutron star interior. It would be possible to study fundamental physics in strong gravitational fields of pulsars and black holes using the SKA and LIGO-India along with other telescopes.

Neutron stars harbour the densest form of matter in its interior. These compact astrophysical objects are unique laboratories for cold and dense matter as these can not be produced in terrestrial laboratories. A wide range of

density, from the density of iron nucleus at the surface of the star to several times normal nuclear matter density (2.7×10^{14} g/cm^3) in the core are expected to be present in neutron stars. The composition and structure of a neutron star are determined by the nature of strong interaction. Several novel phases with large strangeness fraction such as hyperon matter (Glendenning 1992, 1996; Chatterjee & Vidana 2016), Bose–Einstein condensates of strange mesons (Kaplan & Nelson 1986; Pal *et al.* 2000; Banik & Bandyopadhyay 2001a; Knorren *et al.* 1995) and quark matter (Farhi & Jaffe 1984) may appear in the high density regime in neutron stars due to Pauli exclusion principle. Furthermore, the recent accurately measured $2.01 \pm 0.04 M_{\text{solar}}$ neutron star puts stringent condition on the composition and equation of state (EoS) (Antoniadis *et al.* 2013).

On the other hand, there is a growing interplay between the physics of dense matter found in laboratories and neutron stars. Though the quantum chromodynamics (QCD) predicts a very rich phase structure of dense matter, we can only probe a small region of it in laboratories. Relativistic heavy ion experiments produce a hot (a few hundreds MeV) and dense matter (a few times normal nuclear matter density). The study of dense matter in heavy ion collisions reveals many new and interesting results such as the modifications of hadron properties in dense medium, the properties of strange matter including hyperons and (anti)kaons and the formation of quark-gluon plasma (Watts *et al.* 2016; Oertel *et al.* 2017). These empirical information from heavy ion collisions may be useful in understanding dense matter in neutron star interior. The properties of finite nuclei obtained in laboratories such as incompressibility of matter, symmetry energy, etc. also contribute to the understanding of matter in neutron stars.

Extremely high magnetic fields might be produced in heavy ion collisions when moving charges of two heavy nuclei say gold or lead collide with each other at the speed of light. It was estimated that this field could be as high as 10^{19} G (Kharzeev *et al.* 2008). However, such a strong magnetic field is produced for a short time ∼a few fm/c. On the other hand, it was observed that a new class of neutron stars known as magnetars had very strong surface magnetic fields ∼10^{15} G. It was inferred from the virial theorem (Chandrasekhar & Fermi 1953) that the interior magnetic field could be several times higher than the surface fields of magnetars.

This shows that neutron stars are unique laboratories for fundamental physics under extreme densities, magnetic fields and strong gravitational fields. In this article, we describe different phases of matter in supernova

simulations and neutron stars and discuss how compositions and EoS of matter can be constrained from observations. In section 2, theoretical models of EoS in the crust and core are introduced. In connection to SN1987A, the application of this EoS in supernova simulations is elaborated in section 3. Calculations of mass, radius and moment of inertia and their observable consequences are presented in section 4. Matter in strong magnetic fields and oscillatory modes of magnetars are discussed in section 5. Finally conclusions are drawn in section 6.

2. Theoretical modeling of EoS

2.1 *Matter in neutron star crust*

Neutron star interior is broadly separated into two regions – crust and core. Again the crust is divided into the outer crust and inner crust; so is the core. There is a huge variation of matter density starting from 10^4 g/cm^3 in the outer crust to ∼10^{15} g/cm^3 in the core. Consequently, this leads to interesting phases and compositions of matter in different layers of neutron stars. The outer crust is composed of nuclei in the background of a uniformly distributed relativistic electron gas. At around 4×10^{11} g/cm^3, neutrons start dripping out of nuclei when the neutron chemical potential is equal to bare neutron mass. This is the end of the outer crust and the beginning of the inner crust. In this layer of matter, the components of matter are neutron-rich nuclear cluster, free neutrons and a uniform gas of relativistic electron gas. As the density increases, the matter passes through an interesting phase called the pasta phase where various geometrical shapes such as rod, slab, bubble, etc. might appear due to competition between the surface tension and Coulomb interaction in nuclear clusters. It shows that the matter is highly non-uniform in neutron star crusts. Neutron-rich nuclear clusters dissolve into neutrons and protons which, in turn, produce a uniform nuclear matter, at the crust–core interface around the matter density 2.7×10^{14} g/cm^3.

We introduce here the nuclear statistical equilibrium (NSE) model for the description of matter of light and heavy nuclei together with unbound but interacting nucleons at low temperature and mass density below ∼2.7×10^{14} g/cm^3 (Hempel & Schaffner-Bielich 2010). In this model, the nuclear chemical equilibrium is regulated by the modified Saha equation. The total canonical partition function in this model is given by

$$Z(T, V, \{N_i\}) = Z_{\text{nuc}} \prod_{A,Z} Z_{A,Z} \, Z_{\text{Coul}} , \qquad (1)$$

with V denoting the volume of the system. The Helmholtz free energy involving free energies of nucleons (F_{nuc}), nuclei ($F_{A,Z}$) and Coulomb (F_{Coul}) is computed as

$$F(T, V, \{N_i\}) = -T \ln Z \tag{2}$$

$$= F_{nuc} + \sum_{A,Z} F_{A,Z} + F_{Coul} . \tag{3}$$

The number density of each nuclear species (A, Z) is obtained from modified Saha equation (Banik *et al.* 2014)

$$n_{A,Z} = \kappa \, g_{A,Z}(T) \left(\frac{M_{A,Z} T}{2\pi} \right)^{3/2}$$

$$\exp \left(\frac{(A-Z)\mu_n^0 + Z\mu_p^0 - M_{A,Z} - E_{A,Z}^{Coul} - P_{nuc}^0 V_{A,Z}}{T} \right), \tag{4}$$

where $g_{A,Z}$ is the nuclear spin degeneracy; κ is the volume fraction available for nuclei and approaches to zero at the crust–core boundary. Finally one obtains the energy density and pressure in this model.

2.2 *Dense matter in neutron star core*

Neutrons and protons in neutron star core become relativistic as baryon density increases. Furthermore, dense matter in neutron star interior is a highly many body system. The QCD might be the fundamental theory to describe such a dense matter. Here we focus on a relativistic field theoretical model involving baryons and mesons. In this Lorentz covariant theory, baryon–baryon interaction is mediated by the exchanges of mesons. Meson–baryon couplings are made density dependent. Being a relativistic model, this ensures causality in the EoS.

The starting point in the density dependent relativistic hadron (DDRH) field theory is the Lagrangian density which describes baryon–baryon interaction through exchanges of scalar σ, vector ω, ϕ and ρ mesons (Banik *et al.* 2014; Typel *et al.* 2010),

$$\mathcal{L}_B = \sum_B \bar{\psi}_B (i\gamma_\mu \partial^\mu - m_B + g_{\sigma B}\sigma - g_{\omega B}\gamma_\mu \omega^\mu$$

$$- g_{\phi B}\gamma_\mu \phi^\mu - g_{\rho B}\gamma_\mu \boldsymbol{\tau}_B \cdot \boldsymbol{\rho}^\mu) \psi_B$$

$$+ \frac{1}{2}(\partial_\mu \sigma \partial^\mu \sigma - m_\sigma^2 \sigma^2) - \frac{1}{4}\omega_{\mu\nu}\omega^{\mu\nu}$$

$$+ \frac{1}{2}m_\omega^2 \omega_\mu \omega^\mu - \frac{1}{4}\phi_{\mu\nu}\phi^{\mu\nu} + \frac{1}{2}m_\phi^2 \phi_\mu \phi^\mu$$

$$- \frac{1}{4}\boldsymbol{\rho}_{\mu\nu} \cdot \boldsymbol{\rho}^{\mu\nu} + \frac{1}{2}m_\rho^2 \boldsymbol{\rho}_\mu \cdot \boldsymbol{\rho}^\mu. \tag{5}$$

Here ψ_B denotes the baryon octets, $\boldsymbol{\tau}_B$ is the isospin operator and g's are density dependent meson–baryon couplings. It is to be noted that ϕ mesons are mediated between particles having strangeness quantum number.

Next we can calculate the grand-canonical thermodynamic potential per unit volume

$$\frac{\Omega}{V} = \frac{1}{2}m_\sigma^2 \sigma^2 - \frac{1}{2}m_\omega^2 \omega_0^2 - \frac{1}{2}m_\rho^2 \rho_{03}^2$$

$$- \frac{1}{2}m_\phi^2 \phi_0^2 - \Sigma^r \sum_B n_B - 2T$$

$$\times \sum_{i=n,p,\Lambda,\Sigma^-,\Sigma^0,\Sigma^+,\Xi^-,\Xi^0} \int \frac{d^3k}{(2\pi)^3} [\ln(1 + e^{-\beta(E^*-\nu_i)}) + \ln(1 + e^{-\beta(E^*+\nu_i)})], \tag{6}$$

where the temperature is defined as $\beta = 1/T$ and $E^* = \sqrt{(k^2 + m_i^{*2})}$. This involves a term called the rearrangement term Σ^r (Banik *et al.* 2014; Hofmann *et al.* 2001) due to many-body correlations which is given by

$$\Sigma^r = \sum_B [-g'_{\sigma B}\sigma n_B^s + g'_{\omega B}\omega_0 n_B + g'_{\phi B}\phi_0 n_B$$

$$+ g'_{\rho B}\tau_{3B}\rho_{03}n_B + g'_{\phi B}\phi_0 n_B] , \tag{7}$$

where $'$ denotes the derivative with respect to baryon density of species B.

We also study the Bose–Einstein condensation of antikaons (K^- mesons) in neutron star matter. In this case, baryons are embedded in the condensate. We treat the kaon–baryon interaction in the same footing as the baryon–baryon interaction described by the Lagrangian density (5). The Lagrangian density for (anti)kaons in the minimal coupling scheme is (Glendenning & Schaffner-Bielich 1999; Banik & Bandyopadhyay 2001b)

$$\mathcal{L}_K = D_\mu^* \bar{K} D^\mu K - m_K^{*2} \bar{K} K , \tag{8}$$

where K and $\bar{K}$ denote kaon and (anti)kaon doublets; the covariant derivative is $D_\mu = \partial_\mu + ig_{\omega K}\omega_\mu + ig_{\phi K}\phi_\mu + ig_{\rho K}t_K \cdot \rho_\mu$ and the effective mass of (anti)kaons is $m_K^* = m_K - g_{\sigma K}\sigma$. The thermodynamic potential for antikaons is given by

$$\frac{\Omega_K}{V} = T \int \frac{d^3 p}{(2\pi)^3}[\ln(1 - e^{-\beta(\omega_{K^-}-\mu)})$$
$$+ \ln(1 - e^{-\beta(\omega_{K^+}+\mu)})] . \qquad (9)$$

The in-medium energy of K^- meson is given by

$$\omega_{K^-} = \sqrt{(p^2 + m_K^{*2})}$$
$$- \left(g_{\omega K}\omega_0 + g_{\phi K}\phi_0 + \frac{1}{2}g_{\rho K}\rho_{03}\right), \qquad (10)$$

and μ is the chemical potential of K^- mesons and is given by $\mu = \mu_n - \mu_p = \mu_e$. The threshold condition for s-wave ($\mathbf{p} = 0$) K^- condensation is given by $\mu = \omega_{K^-} = m_K^* - g_{\omega K}\omega_0 - g_{\phi K}\phi_0 - \frac{1}{2}g_{\rho K}\rho_{03}$. Mean field values of mesons are σ, ω_0, ϕ_0 and ρ_{03}.

Thermodynamic quantities like energy density, pressure, etc. in the hadronic and kaon condensed phases are computed from the grand-thermodynamic potentials (Banik *et al.* 2008, 2014; Char & Banik 2014). Charge neutrality and β-equilibrium constraints are imposed on neutron star matter.

Finally, meson-nucleon density dependent couplings are obtained by fitting properties of finite nuclei (Banik *et al.* 2014; Typel *et al.* 2010). Vector meson couplings for hyperons and kaons are estimated theoretically using the symmetry relations (Weissenborn *et al.* 2012; Schaffner & Mishustin 1996) whereas their scalar couplings are obtained from hyeprnuclei and kaonic atom data (Char & Banik 2014).

Recently, Banik, Hempel and Bandyopadhyay (BHB) constructed a hyperon EoS for supernova and neutron star matter involving Λ hyperons and the repulsive $\Lambda-\Lambda$ interaction mediated by ϕ mesons (Banik *et al.* 2014). This hyperon EoS is compatible with $2M_{solar}$ neutron stars and is denoted by BHB$\Lambda\phi$ (Banik *et al.* 2014).

In the following sections, we describe the role of compositions and EoS on the evolution of the PNS in core collapse supernova simulations, masses, radii and moments of inertia of neutron stars and magnetoelastic oscillations of strongly magnetized neutron stars.

3. Mystery of the missing compact star in SN1987A

Over the past thirty years, SN1987A has been the most studied core-collapse supernova event. It is the only supernova event from which neutrinos were detected

after the explosion over 11 s. It was evident from the detection of neutrinos that a hot and neutrino-trapped protoneutron star was born and existed for about 11 s. There is no detection of a neutron star in SN1987A so far. It is believed that an event horizon was formed after 11 s and the PNS collapse into a black hole. The question is what made the PNS metastable and drove it into a black hole.

Different groups investigated the problem of stability of a PNS for short times. When a PNS is made up of nucleons and leptons, it has a slightly smaller maximum mass than that of the neutron star. However, this situation changes with the appearance of exotic matter such as hyperons or K^- condensation in dense matter during the evolution of the PNS (Banik 2014; Brown & Bethe 1994). The PNS including hyperon and/or Bose–Einstein condensate has a higher maximum mass than that of a cold neutron star (Brown & Bethe 1994; Prakash *et al.* 1995; Banik & Bandyopadhyay 2001b). Neutrino and thermal pressure could stabilize much larger maximum mass for a protoneutron star during the evolution. However, the PNS might be unstable after de-leptonization and cooling.

The role of Λ hyperons on supernova explosion mechanism and the evolution of PNS has been studied using a general relativistic one-dimensional core collapse supernova model (O'Connor & Ott 2011). Earlier simulations were done with the hyperon EoS which was not compatible with the two solar mass neutron star (Banik 2014). Furthermore, the long duration evolution of the PNS with enhanced neutrino heating in the supernova simulation with 23 solar mass progenitor is denoted as s23WH07 and is investigated to test the hypothesis of metastability in the PNS. The Λ hyperon EoS of Banik, Hempel and Bandyopadhyay, BHB$\Lambda\phi$ is used as microphysical input in this simulation. Λ hyperons appear just after core bounce and its population became significant as the PNS evolves. This simulation leads to a successful supernova explosion and the PNS evolves to a stable neutron star of $2.0M_{solar}$ over 3 s as is evident from Fig. 1. This is compared with the result of our earlier CCSN simulation of $20M_{solar}$ progenitor denoted as s20WH07 that led to a stable neutron star of $1.6M_{solar}$ (Char *et al.* 2015). These findings are at odds with the prediction about the collapse of the PNS into a black hole after de-leptonization and cooling.

4. Probing neutron star interior: Mass, radius and moment of inertia

Neutron star masses have been estimated to very high degree of accuracy due to the measurement of
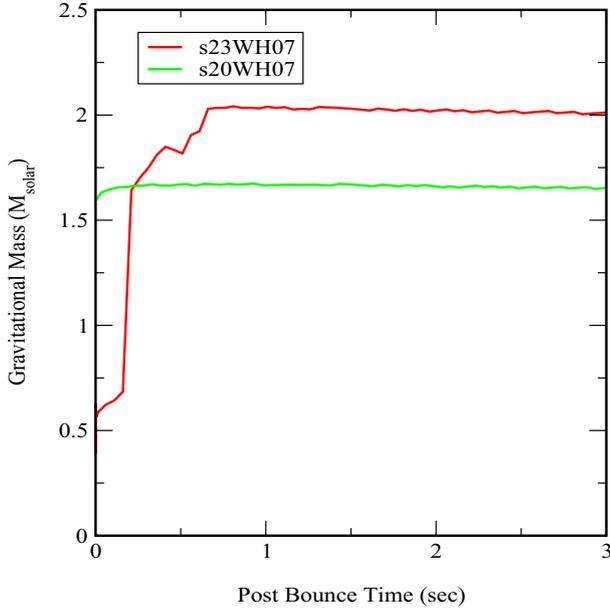
Figure 1. Long duration evolution of the protoneutron star using 20 and $23 M_{\text{solar}}$ progenitors and BHB$\Lambda\phi$ EoS.

post-Keplerian parameters in relativistic binary systems. The accurately measured highest neutron star mass (M) is $2.01 \pm 0.04 M_{\odot}$ so far. However, the estimation of radius from observations is still problematic (Bhattacharyya *et al.* 2017). The discovery of highly relativistic binary systems such as the double pulsar system PSR J0737-3039 for which masses of both pulsars are known accurately, opens up the possibility for the determination of moment of inertia (I) of pulsar A which, in turn, might overcome the uncertainties in the determination of radius (R). It is expected that the high precision timing technique in the upcoming SKA would facilitate the extraction of the moment of inertia of a pulsar earlier than that in the present day scenario. Higher order post-Newtonian (PN) effects in relativistic neutron star binaries could be probed in the SKA era. Furthermore, the relativistic spin-orbit (SO) coupling might result in an extra advancement of periastron above the PN contributions. The measurement of the SO coupling effect over and above the contribution of the second PN term could lead to the determination of moment of inertia of a pulsar in relativistic neutron star binaries in general (Damour & Schaefer 1988) and the double pulsar system in particular (Lattimer & Schutz 2005). Observed masses, radii and moments of neutrons are direct probes of compositions and EoS in neutron star interior. The theoretical mass-radius, moment of inertia – compactness parameter (ratio of mass and radius) relationships of neutron stars could be directly compared with measured masses, radii and moments of inertia from various

observations. Observations indicate that neutron stars are slowly rotating and the fastest rotating neutron star among them has a frequency of 716 Hz. Structures of non-rotating neutron stars are computed from the Tolman–Oppenheimer–Volkoff (TOV) equation

$$
\frac{\mathrm{d}p}{\mathrm{d}r} = -\frac{G\varepsilon(r)m(r)}{c^2 r^2}\left(1 + \frac{p(r)}{\varepsilon(r)}\right)\left(1 + \frac{4\pi r^3 p(r)}{m(r)c^2}\right)
$$
$$
\times \left[1 - \frac{2Gm(r)}{c^2 r}\right]^{-1}. \tag{11}
$$

We need an EoS to close the TOV equation.

Slowly rotating neutron stars are investigated by perturbing the spherical space-time metric (Hartle & Thorne 1968). Moment of inertia is calculated from $I = J/\Omega$, where

$$
I = \frac{8\pi}{3}\int_0^R r^4 e^{(\lambda-\nu)}\left(p(r) + \varepsilon(r)\right)\frac{(\Omega - \omega(r))}{\Omega}\mathrm{d}r, \tag{12}
$$

and the frame-dragging angular velocity (ω) is obtained by solving the Hartle equation; Ω is the spin of the neutron star and λ, ν are metric functions.

We consider different compositions for the computation of EoS, mass–radius relationship and moment of inertia. Neutron star matter made of neutrons and protons is denoted by np. In this calculation, Λ hyperons appear first at baryon density $n_b = 2.2n_0$ where the saturation density is $n_0 = 0.149$ fm^{-3}. The repulsive Λ–Λ interaction is mediated by ϕ mesons. This composition of matter involving neutrons, protons and Λ hyperons is represented by $np\Lambda\phi$. Being heavier, Σ and Ξ hyperons are populated at much higher densities and excluded from this calculation. Another exotic phase of matter considered here is the Bose–Einstein condensed matter of K^- mesons in which neutrons, protons and Λ hyperons are embedded in the condensate and is denoted by $np\Lambda K^-\phi$. The threshold density for K^- condensation is obtained from the equality of in-medium energy (ω_{K^-}) of K^- and electron chemical potential (μ_e). This is exhibited in Fig. 2. In this case, the onset of the condensate occurs at $n_b = 3.69n_0$.

Figure 3 shows the relation between pressure (P) and energy density (ε) which is known as the EoS, for the above mentioned compositions of matter. It is evident from the figure that additional degrees of freedom in the form of hyperons and K^- condensate make an EoS softer. This is also reflected in the structures of neutron stars. Mass-radius relationships for different compositions and EoS are shown in Fig. 4. Being the stiffest among all other cases considered here,
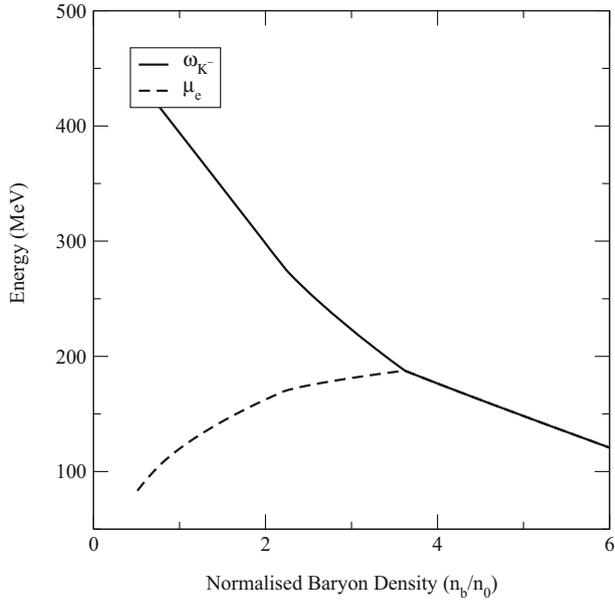
Figure 2. In-medium energy of K^- mesons (ω_{K^-}) and electron chemical potential (μ_e) as a function of normalized baryon density.
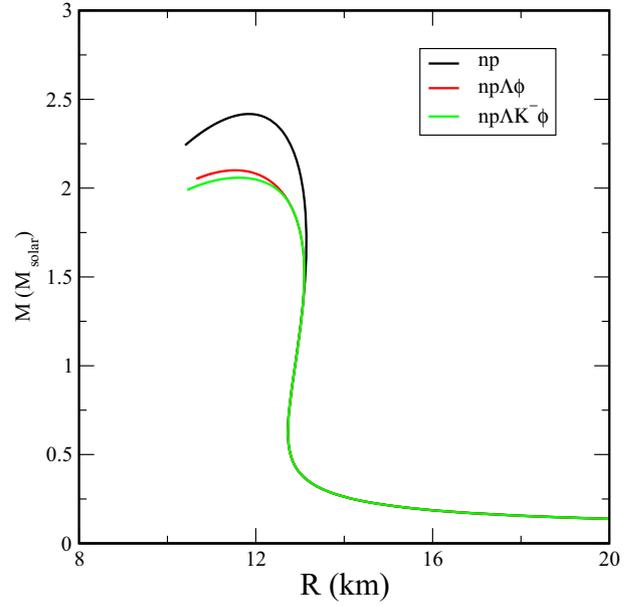
Figure 4. Mass–radius relationship for neutron star compositions np, $np\Lambda\phi$ and $np\Lambda K^-\phi$.
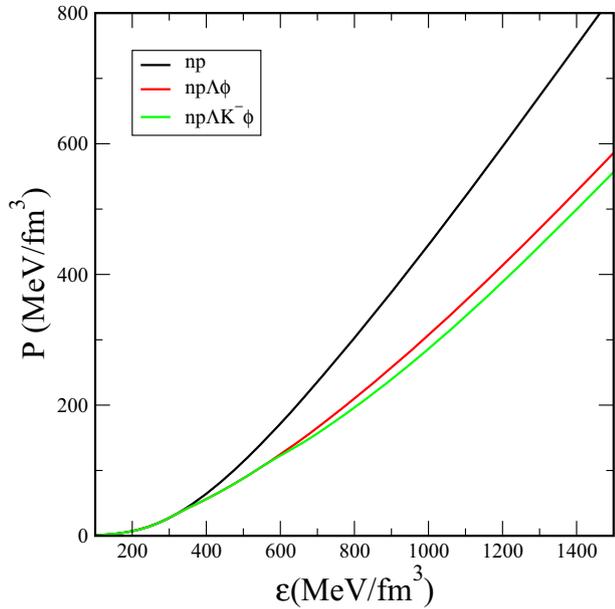
Figure 3. Pressure as a function of energy density for compositions np, $np\Lambda\phi$ and $np\Lambda K^-\phi$.
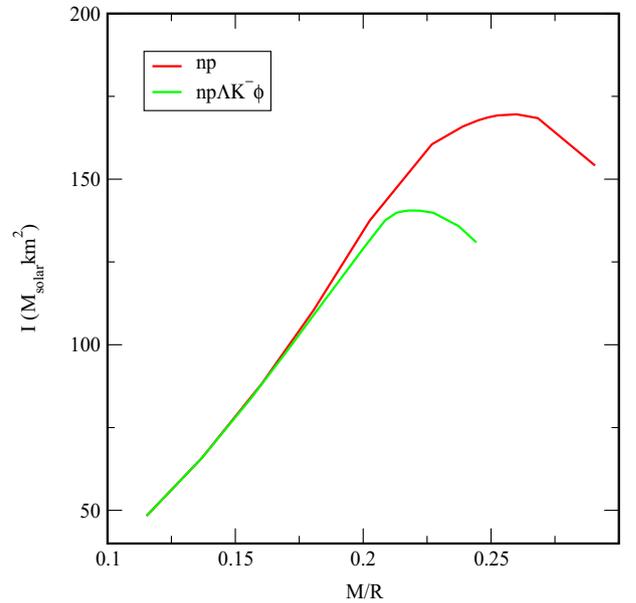
Figure 5. Moment of inertia versus compactness for neutron star compositions np and $np\Lambda K^-\phi$.

nuclear matter EoS results in the highest maximum mass neutron star of $2.42M_{\rm solar}$. On the other hand, Λ hyperons and K^- condensate make the EoS softer leading to smaller maximum mass neutron stars. The maximum mass corresponding to $np\Lambda\phi$ case is $2.1M_{\rm solar}$, whereas it is $2.09M_{\rm solar}$ for the $np\Lambda K^-\phi$ case. It is important to note that for exotic phases of matter maximum masses are well above the observational benchmark of

$2.01\pm0.04M_{\rm solar}$. It demonstrates that there is room for exotic matter in neutron star interior. Moment of inertia is plotted against the compactness parameter (M/R) in Fig. 5. It is evident from the figure that the moment of inertia corresponding to nuclear matter EoS is significantly higher than that of the Bose–Einstein condensed matter for compactness above 0.2. If the moment of inertia of pulsar A in the double pulsar is estimated in

future, the radius could be determined for this pulsar because its mass is already known accurately (Lattimer & Schutz 2005).

5. Neutron star matter in strong magnetic fields

Neutron star crust plays an important role in many observational phenomena, for example, cooling of neutron stars, glitches and Quasi Periodic Oscillations (QPOs). Heat transport and magnetic field evolution in the crust are sensitive to the composition of the crust. Similarly, the shear modulus which is an important input in understanding QPOs believed to be magnetoelastic oscillations, is impacted by the crustal composition. On the other hand, superfluid neutrons in the crust might be responsible for pulsar glitches.

It was observed that a class of neutron stars called magnetars has surface magnetic fields as large as 10^{15} G. Soft Gamma Repeaters (SGRs) and Anomalous X-ray Pulsars (AXPs) are thought to be very good candidates of magnetars (Duncan & Thompson 1992; Duncan 1998, Kouveluotou *et al.* 1998). SGRs exhibited giant flares of gamma rays in several instances. QPOs were observed in the decaying tails of giant flares in SGR 0526-66, SGR 1900+14 and SGR 1806-20 caused by the magnetic field evolution and its impact on the crust.

It was argued that the interior magnetic field could be several orders of magnitude higher than the surface field of magnetars. The flux conservation in core collapse supernovae and virial theorem (Chandrasekhar & Fermi 1953) predict a maximum interior magnetic field of $\sim 10^{18}$ G without causing any instability in the star. Like a density gradient from the surface to the centre, the magnetic field should show a similar behaviour as described by the ansatz (Bandyopadhyay *et al.* 1997)

$$B_m(n_b/n_0) = B_m^{surf} + B_0[1 - \exp\{-\beta(n_b/n_0)^\gamma\}].$$
$$(13)$$

Several groups studied the influence of strong magnetic fields on the compositions and EoS of neutron star matter and its observable consequences (Chakraborty *et al.* 1997; Bandyopadhyay *et al.* 1997, 1998; Broderick *et al.* 2000; Lai 2001; Nandi *et al.* 2016). Such a strong magnetic field is expected to influence charged particles such as electrons in the crust through Landau quantization. As no free protons are available in the crust, protons are not Landau quantized. However, protons are affected through charge neutrality. Number density, energy density and
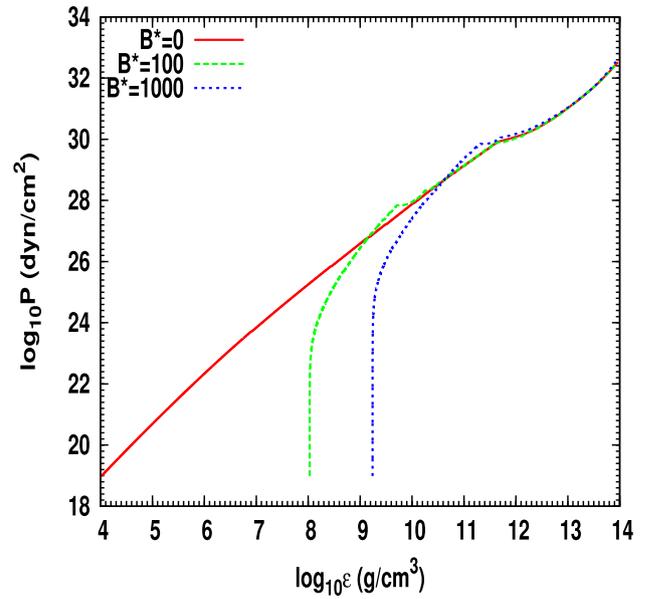
Figure 6. EoS of neutron star crust with and without magnetic field.

pressure of relativistic electrons are influenced by the phase space modifications of electrons due to Landau quantization. Here we adopt the Baym, Pethick and Sutherland (BPS) model of the outer crust (Nandi & Bandyopadhyay 2011) and the inner crust model of Nandi *et al.* (2011) in the presence of strong magnetic fields. In Fig. 6, pressure is plotted as a function of energy density for the crust with and without magnetic fields. Here the magnetic field strength is given in terms of the critical field (B_c) for electrons i.e. $B = B_* B_c$ where $B_c = 4.414 \times 10^{13}$ G. It is observed from the figure that the EoS of the crust in the presence of strong magnetic fields is significantly modified in the energy density regime $<10^{10}$ g/cm^3 due to the population of electrons in the zeroth Landau level compared to the zero field case ($B_* = 0$). However, several Landau levels are populated in the high density regime above 10^{10} g/cm^3. Consequently, results of $B_* = 100, 1000$ approach the classical result without magnetic field.

This magnetized crust model is applied to the problem of magnetoelastic oscillations in magnetars to explain QPOs in giant flares (Nandi *et al.* 2016). In contrast to the state-of-the-art general relativistic magnetohydrodynamics (Gabler *et al.* 2012), our calculation is based on a general relativistic spherical symmetric model of neutron stars with dipole magnetic fields and involves crust–core coupling. Two situations are considered for magnetoelastic modes. In one case, magnetoelastic modes confined to the crust (CME) are relevant. In the other case, global magnetoeleastic (GME) modes become important when the crust–core

coupling is considered. For magnetic fields $> 10^{15}$G, the Alfvén velocity becomes greater than the shear velocity. Consequently, GME mode frequencies just become those of pure Alfvén modes.

Detections of fundamental and first overtone frequencies in SGR 1806-20 giant flare could constrain the EoS. This can lead to the determination of the crust thickness. It was shown that the crust thickness might be estimated from the ratio of fundamental and first overtone frequencies (Sotani *et al.* 2007) $\frac{\Delta R}{R} = {}_l C^n \frac{{}_l f^0}{{}_l f^n}$. It is also evident from this relation that the crust thickness is inversely proportional to the frequency of higher harmonics. One can estimate the crust thickness taking 18 Hz as the fundamental frequency (${}_l f^0$) and 626 Hz as the first overtone frequency (${}_l f^1$). This led to a ratio of 0.06 with ${}_l C^n \sim 2$ which favoured a stiff EoS model (Sotani *et al.* 2007). It was noted that the radius of a neutron star increased in strong magnetic fields compared with the zero-field case. Consequently, the thickness of the crust increased in strong fields (Nandi *et al.* 2016). We obtain a crust thickness of 0.088 km and the value of ${}_l C^1$ is 3.06 for the magnetized EoS as shown in Fig. 6. Such a description relating the crust thickness to the ratio of observed frequencies is relevant for CME modes. The effects of magnetized crusts on magnetoelastic modes disappear above a critical field of 4×10^{15} G. Furthermore, GME modes might explain all frequencies of SGR 1806-20.

6. Conclusions and outlook

We have demonstrated through core collapse supernova simulations and calculation of neutron star structures that EoSs involving exotic components of matter such as hyperons and/or Bose–Einstein condensates are compatible with $2M_{\text{solar}}$ neutron stars. Determination of moment of inertia of a neutron star in relativistic neutron star binaries in the SKA era would allow the simultaneous measurements of mass and radius of a particular neutron star. The model independent construction of an EoS might be possible if masses and radii of same neutron stars are known (Lindblom 1992). This is one of several spin offs of the knowledge of moment of inertia. The superfluid phase in pulsar glitches is another interesting area of investigation. The entrainment effect in the superfluid matter could severely constrain the reservoir of superfluid moment of inertia in the crust (Andersson *et al.* 2012). The recent discovery of negative effective mass in a Bose–Einstein condensate makes this study more interesting and challenging (Khamehchi *et al.* 2017). It is to be seen what

is the role of negative effective mass on the superfluid hydrodynamics in neutron stars and its connection to glitch phenomena.

References

Andersson, N., Glampedakis, K., Ho, W. C. G., Espinoza, C. M. 2012, *Phys. Rev. Lett*. **109**, 241103.

Antoniadis, J. *et al.* 2013, *Science*, **340**, 448.

Baade, W., Zwicky, F. 1934, *Phys. Rev.*, **45**, 138.

Bandyopadhyay, D., Chakraborty, S., Pal, S. 1997. *Phys. Rev. Lett.*, **79**, 2176

Bandyopadhyay, D., Chakraborty, S., Dey, P., Pal, S. 1998, *Phys. Rev.*, **D58**, 121301.

Banik, S., Bandyopadhyay, D. 2001, *Phys. Rev.*, **C63**, 035802.

Banik, S., Bandyopadhyay, D. 2001, *Phys. Rev. C* **64**, 055805.

Banik, S., Greiner, W., Bandyopadhyay, D. 2008, *Phys. Rev.*, **C78**, 065804.

Banik, S., Hempel, M., Bandyopadhyay, D. 2014, *ApJS*, **214**, 22.

Banik, S. 2014, *Phys. Rev.*, **C89**, 035807.

Bhattacharyya, S., Bombaci, I., Bandyopadhyay, D., Thampan, A. V., Logoteta, D. 2017, *New Astronomy*, **54**, 61

Brown, G. E., Bethe, H. A. 1994, *ApJ*, **423**, 659.

Broderick, A., Prakash, M., Lattimer, J. M. 2000, *ApJ*, **537**, 351.

Chakraborty, S., Bandyopadhyay, D., Pal S. 1997, *Phys. Rev. Lett.*, **78**, 2898.

Chandrasekhar, S., Fermi, E. 1953, *ApJ*, **118**, 116.

Char, P., Banik, S. 2014, *Phys. Rev. C* **90**, 015801.

Char, P., Banik, S., Bandyopadhyay, D. 2015, *ApJ*, **809**, 116.

Chatterjee, D., Vidana, I. 2016, *Eur. Phys. J.*, **A52**, 29.

Damour, T., Schaefer, G. 1988, *Nuovo Cimento*, **B101**, 127.

Duncan, R. C., Thompson, C. 1992, *ApJ*, **392**, L9.

Duncan, R. C. 1998, *ApJ*, **498**, L45.

Farhi, E., Jaffe, R. L. 1984, *Phys. Rev. D* **30**, 2379.

Gabler, M., *et al.* 2012, *MNRAS*, **421**, 2054.

Glendenning, N. K., Schaffner-Bielich, J. 1999, *Phys. Rev. C* **60**, 025803.

Glendenning, N. K. 1992, *Phys. Rev*. **D46**, 1274.

Glendenning, N. K. 1996, *Compact Stars : Nuclear Physics, Particle Physics and General Relativity*, Springer-Verlag, New York.

Hartle, J. B., Thorne, K. S. 1968, *ApJ*, **153**, 807.

Hempel, M., Schaffner-Bielich, J. 2010, *Nucl. Phys.*, **A837**, 210.

Hewish, A., Bell, S. J., Pilkington, J. D. H., Scott, P. F., Collins, R. A. 1968, *Nature*, **217**, 709.

Hofmann, F., Keil, C. M., Lenske, H. 2001, *Phys. Rev.*, **C64**, 025804.

Kaplan, D. B., Nelson, A. E. 1986, *Phys. Lett.*, **B175**, 57.

Khamehchi, M. A., Hossain, K., Mossman, M. E., Zhang, Y. 2017, *Phys. Rev. Lett.*, **118**, 155301.

Kharzeev, D. E., McLerran, L. D., Warringa, H. J. 2008, *Nucl. Phys.*, **A803**, 227.

Knorren, R., Prakash, M., Ellis, P. J. 1995, *Phys. Rev.*, **C52**, 3470.

Konar, S. *et al.* 2016, *J. Astrophys. Astr.* **37**, 36.

Kouveluotou, C. *et al.* 1998, *Nature*, **393**, 235.

Lai, D. 2001, *Rev. Mod. Phys.*, **73**, 629.

Landau, L. D. 1932, *Phys. Zs. Sowjet.*, **1**, 285.

Lattimer, J. M., Schutz, B. F. 2005, *ApJ*, **629**, 979.

Lindblom, L. 1992, *ApJ*, **398**, 569.

Nandi, R., Bandyopadhyay, D. 2011, *J. Phys. Conf. Ser.*, **312**, 042016.

Nandi, R., Bandyopadhyay, D., Mishustin, I. N., Greiner, W. 2011, *ApJ*, **736**, 156.

Nandi R., Char P., Chatterjee D., Bandyopadhyay D., 2016, *Phys. Rev.*, **C94**, 025801.

O'Connor, E., Ott, C. D. 2011, *ApJ*, **730**, 70.

Oertel, M., Hempel, M., Klähn, T., Typel, S. 2017, *Rev. Mod. Phys.*, **89**, 015007.

Pal, S., Bandyopadhyay, D., Greiner, W. 2000, *Nucl. Phys.*, **A674**, 553.

Prakash, M., Cooke, J. R., Lattimer, J. M. 1995, *Phys. Rev.*, **D52**, 661.

Schaffner, J., Mishustin, I. N. 1996, *Phys. Rev.*, **C53**, 1416.

Sotani, H., Kokkotas, K. D., Stergioulas, N. 2007, *MNRAS*, **375**, 261.

Typel, S., Röpke, G., Klähn, T., Blaschke, D. 2010, *Phys. Rev.*, **C81**, 015803.

Yakovlev, D. G., Haensel, P., Baym, G., Pethick, C. 2013, *Phys. Uspecki*, **56**, 289.

Watts, A. L., Chakrabarty, D., Feroci, M., Hebeler, K. 2016, *Rev. Mod. Phys.*, **88**, 021001.

Weissenborn, S., Chatterjee, D., Schaffner-Bielich, J. 2012, *Nucl. Phys.*, **A881**, 62.